

Inertial particle motion in a Taylor Couette rotating filter

Steven T. Wereley and Richard M. Lueptow

Department of Mechanical Engineering, 2145 Sheridan Road, Northwestern University, Evanston, Illinois 60208

(Received 26 May 1998; accepted 16 October 1998)

In rotating filtration, which is based on supercritical cylindrical Couette flow with a rotating porous inner cylinder, the motion of particles in the suspension depends on both centrifugal sedimentation and transport due to the vortical motion of Taylor vortices. We have simulated the motion of dilute, rigid, spherical particles in Taylor Couette flow using computational particle tracking in an analytic velocity field for flow just above the transition to supercritical Taylor vortex flow. Neutrally buoyant particles follow fluid streamlines closely, but not exactly due to the curvature of the velocity field very near the particle. The motion of particles with a density greater than the fluid is primarily determined by the competition between the centrifugal sedimentation related to the primary cylindrical Couette flow and the secondary radial and axial transport of the Taylor vortex flow. As a result, particles that start near the outer edge of a vortex spiral inward toward a limit cycle orbit. Likewise, particles initially near the center of a vortex spiral outward toward the same limit cycle orbit. Even when a small radially inward throughflow is imposed, particles can remain trapped in retention zones that are away from the wall of the annulus. Consequently, the dynamics of the flow field result in particles tending to be transported away from the porous inner cylinder, thus contributing to the antiplugging character of rotating filter devices. © 1999 American Institute of Physics. [S1070-6631(99)01302-1]

I. INTRODUCTION

A rotating filter separator consists of a porous inner cylinder rotating within an outer cylindrical shell. As a suspension travels axially in the annulus, filtrate is withdrawn through the inner cylinder, leaving an increasingly concentrated suspension in the annulus. Rotating filters are presently used for the separation of plasma from whole blood and other biological separations, and they show promise for a wide range of other filtration applications. The unique advantage of rotating filtration is that plugging of the pores of the filter with particles is greatly reduced compared to standard filtration techniques. Three mechanisms have been proposed for this resistance to fouling.¹ First, Taylor vortices may “scrub” the filter surface, washing off particles that could potentially plug the filter pores.² Second, since the particulate phase is typically more dense than the fluid, the centrifugal field in the annulus resulting from the rotation of the filter may cause significant sedimentation of particles away from the filter surface. Third, the rotation of the filter gives rise to a high shear, much like that in cross-flow filtration, which has been shown to enhance flow through a filter medium due to shear-induced particle migration away from the filter surface.³ In this paper, we computationally track particles in Taylor Couette flow in order to investigate the role of the first two mechanisms with respect to the antiplugging character of rotating filters.

A significant body of research related to rotating filter separation exists,^{1,2,4-10} but most of these studies were focused on the filtration performance in specific applications, with little attention paid to the physics of the particle motion in a rotating filter. The flow field in a rotating filter is quite

complex and is best described as supercritical cylindrical Couette flow in an annulus with a porous wall boundary condition at the inner cylinder and a superimposed axial flow. The rotation of the inner cylinder creates a centrifugal field that is a maximum near the inner rotating cylinder and decreases to zero at the stationary outer cylinder. This centrifugal field creates a net radial force on non-neutrally buoyant particles. At the same time the toroidal Taylor vortices carry particles from near the inner cylinder to near the outer cylinder, and vice versa. The axial flow carries particles along the length of the rotating filter annulus, while the flow through the porous wall of the inner cylinder carries particles radially inward.

The motion of individual particles in Taylor vortex flow has not been investigated in detail, except for the notable computational particle tracking of Rudman and co-workers.^{11,12} They computationally placed particles in both nonwavy and wavy vortex flow fields calculated using finite difference methods and then tracked inertial particles in the flow field. Although they provided some information on particle paths, their primary interest was the strain history that inertial particles experienced due to their paths and the dispersion of fluid particles. While our approach is similar to Rudman and co-workers, in that we also computationally track particles in Taylor vortex flow, there are significant differences. First, our focus is on the segregation of particles as a result of interaction of Taylor vortices with the centrifugal field. Second, by considering various particle densities, we attempt to describe the underlying physics of the segregation. Third, we consider the effect of an imposed net radial flow, which is inherently present in a rotating filter, on the

particle motion. Fourth, we use an analytic representation of the fluid velocity field rather than a computationally determined flow field.

II. TAYLOR VORTEX FLOW MODEL AND PARTICLE TRACKING

We model the flow in a rotating filter separator as non-wavy, nonhelical Taylor vortex flow. The axial velocity due to axial throughflow is usually only a few percent of the surface speed of the rotating filter.^{13,14} As a result, the axial Reynolds numbers are typically small enough so that the net effect of the imposed axial flow is simply the axial translation of nonwavy vortices without the appearance of helical vortices that occur at higher axial Reynolds numbers.^{13,15-18} Consequently, the axial through-velocity can be neglected with regard to its effect on particle motion within vortices. Its only effect is to carry particles axially with the axially translating vortices. Initially, we also neglect the radial velocity through the porous inner cylinder, since it is typically two orders of magnitude smaller than the velocities arising from the Taylor vortices.^{1,13} In Sec. IV we will include the effect of an imposed inward radial flow at the inner cylinder.

The Taylor vortex velocity field was modeled by Davey¹⁹ using a weakly nonlinear perturbation solution of the Navier–Stokes equations that provides a continuous representation of the velocity field that matches experimental data quite well.^{14,20-23} The first two terms of the velocity components are usually adequate to accurately model the flow.^{14,23} The velocity components, normalized with the speed of the inner cylinder $r_i\Omega$, are

$$u_r(r, z, \epsilon') = A_e(\epsilon')u_1(r)\cos kz + A_e^2(\epsilon')u_2(r)\cos 2kz, \tag{1a}$$

$$\begin{aligned} u_\theta(r, z, \epsilon') = & A_0r + B_0/r + A_e^2(\epsilon')\bar{v}_1(r) \\ & + A_e(\epsilon')v_1(r)\cos kz \\ & + A_e^2(\epsilon')v_2(r)\cos 2kz, \end{aligned} \tag{1b}$$

$$u_z(r, z, \epsilon') = A_e(\epsilon')w_1(r)\sin kz + A_e^2(\epsilon')w_2(r)\sin 2kz, \tag{1c}$$

where $\epsilon' = 1 - (\text{Re}_c/\text{Re})^2$, A_e is a generalized amplitude coefficient, u_n , v_n , and w_n are shape factors (eigenfunctions of the linear stability problem), and k is the fundamental axial wave number. Here $\text{Re} = r_i\Omega d/\nu$ is the rotating Reynolds number based on the radius of the inner cylinder r_i , the rate of rotation Ω , the gap between the cylinders d , and the kinematic viscosity ν . Also, Re_c is the critical rotating Reynolds number at which the transition to supercritical flow occurs. Note that the azimuthal velocity includes the stable flow solution $A_0r + B_0/r$ along with a correction to the mean velocity $\bar{v}_1(r)$. Here A_e , k , u_n , v_n , w_n , and \bar{v}_1 were found following the solution method outlined by Davey.

The motion of a rigid, spherical particle of radius a in a dilute suspension can be well described by a form of Newton's second law of Maxey and Riley,²⁴

$$\begin{aligned} m_p \frac{dV_i}{dt} = & m_f \left. \frac{Du_i}{Dt} \right|_{Y(t)} - \frac{1}{2} m_f \frac{d}{dt} \left(V_i(t) - u_i[Y(t), t] \right. \\ & \left. - \frac{1}{10} a^2 \nabla^2 u_i|_{Y(t)} \right) + (m_p - m_f)g_i \\ & - 6\pi a \mu \left(V_i(t) - u_i[Y(t), t] - \frac{1}{6} a^2 \nabla^2 u_i|_{Y(t)} \right), \end{aligned} \tag{2}$$

where m_p is the mass of the particle, m_f is the mass of the fluid displaced by the particle, $Y(t)$ is the location of the particle, V_i is the velocity of the particle, u_i is the velocity field of the fluid from Eq. (1), and μ is the dynamic viscosity of the fluid. The left side of the equation represents the inertia of the particle. The terms on the right side are, from left to right, the pressure gradient force (called this since the fluid acceleration is related to the pressure gradient of the undisturbed flow), the added mass force (related to the necessity of moving a mass of fluid when a particle displaces it), the gravitational body force, and the Stokes drag force. The Basset history force, which is important in the initial motion of a particle starting from rest under certain conditions, can be neglected, since other acceleration terms are much larger for the long-time behavior of the particles. The Laplacian of the velocity field, known as the Faxen correction, was included in two terms on the right side of Eq. (2) by Maxey and Riley to correct for the effects of curvature in the velocity field on the drag force, assuming steady Stokes flow around a sphere.²⁴ The Coriolis and centrifugal accelerations acting on the particle do not explicitly appear in Eq. (2), but appear implicitly in the terms containing the particle velocity V_i when properly accounting for the rotating frame of reference. A shortcoming of using Eq. (2) is that it is based on creeping flow, so it does not include lateral migration of the particle due to Saffman lift related to the velocity shear or wall effects. Using a modified lift expression,²⁵ it can be shown that the lift is at least an order of magnitude smaller than the drag force. Likewise, the wall effects can be shown to be about an order of magnitude smaller than the drag when the particles are more than one to two diameters from the wall.²⁶ Consequently, we ignore these effects. A conventional finite difference discretization of Eq. (2) was used to integrate the particle's position and velocity forward in time using a standard Runge–Kutta technique with Eq. (1) used for the velocity field of the fluid.

Several parameters are important for the simulation. The cylinder radius ratio was set to $\eta = r_i/(r_i + d) = 0.83$, to correspond to the radius ratio for which we typically perform experiments. For this radius ratio, the vortex pair spacing, based on k determined as part of the Davey solution, is $2.007d$. The rotating Reynolds number was set to $\text{Re} = 125$, which is above the Reynolds number for transition to Taylor Couette flow of $\text{Re}_c = 102$ for this radius ratio, but below the Reynolds number for the transition to wavy vortex flow of $\text{Re} \approx 130$. The Davey solution has been shown to closely match experimentally measured Taylor Couette velocity fields under these conditions.^{14,23} There are two important parameters for the particles that are being tracked: the density ratio, $\beta = \rho_p/\rho_f$, where ρ_p is the particle density and ρ_f is the fluid density; and the particle size ratio, $\alpha = d/2a$.

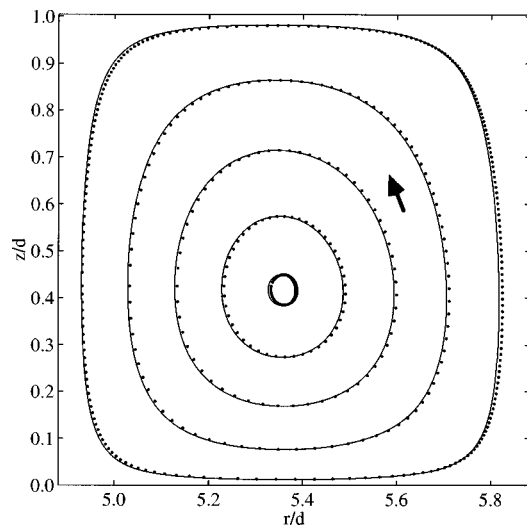


FIG. 1. Neutrally buoyant particle paths projected in a meridional plane for a counterclockwise vortex. Dots represent particle positions at equally spaced time instants, while the solid curves represent the best fit streamline to each set of dots.

III. MOTION OF PARTICLES IN TAYLOR COUETTE FLOW

Although our primary interest is in the balance of forces on particles that are more dense than the fluid, it is helpful to first consider the motion of a neutrally buoyant particle of finite size, as opposed to an infinitely small fluid particle. For a neutrally buoyant particle, the gravitational term in Eq. (2) drops out. But the particle's velocity, V_i , cannot be identical to the surrounding fluid velocity, u_i , because of the Laplacian (the Faxen correction to account for the effects of curvature in the velocity field) in the added mass term and the Stokes drag force term. Carrying out the analysis indicates that the added mass term is negligible in comparison to the other terms, so it is the Laplacian in the drag term that results in the particle velocity differing from the fluid velocity.

The effect of the correction to the drag force is quite small, but readily evident when comparing the fluid streamlines with the particle paths, as shown in Fig. 1. In this and subsequent figures, the horizontal coordinate is the radial coordinate normalized by the gap width, r/d , so that the wall of the inner rotating cylinder is the left side of the figure and the wall of the outer fixed cylinder is the right side of the figure. The vertical coordinate is the axial position normalized by the gap width, z/d , with $z=0$ corresponding to an outflow boundary between vortices. Thus, we show a single counterclockwise vortex. The particle paths and streamlines indicated in the figure are projections in the meridional plane. The actual paths and streamlines also have an azimuthal component (into the page) that is not shown. Five particle paths are represented by dots corresponding to uniformly spaced time increments in Fig. 1. The streamlines are a best fit to the corresponding particle path (in a least-squares sense). The particle paths are nearly aligned with the streamlines at the top and the bottom of the orbits, corresponding to inflow and outflow boundaries of the vortices. But the particle paths are slightly outward from the streamlines during

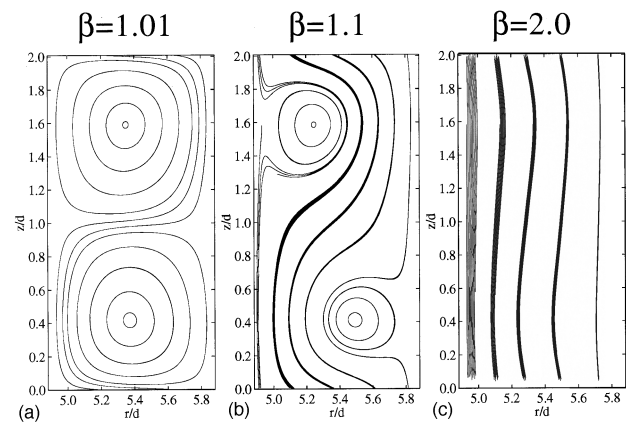


FIG. 2. Particle paths projected in the meridional plane with gravity acting downward for $Re=125$ and $\alpha=29.7$. The upper vortex rotates CW; the lower vortex rotates CCW. (a) $\beta=1.01$; (b) $\beta=1.1$; (c) $\beta=2.0$.

the axial portion of the orbit due to the correction of the drag force. Particles retrace their orbits to within the accuracy of the simulation for the length of the simulation, which was several hundred revolutions around the vortex center.

While the particles travel around the center of the vortex as shown in Fig. 1, the azimuthal velocity of the fluid carries the particles azimuthally at a very high speed near the inner cylinder and at a very low speed near the outer cylinder. As a result, a particle on the outer orbit is continually accelerating to high azimuthal velocity near the inner cylinder and then decelerating to a low azimuthal velocity near the outer cylinder as it traces its orbit. On the other hand, a particle on the innermost orbit sees nearly the same azimuthal velocity throughout its orbit. At the Reynolds number for which this simulation was run, the particle on the outermost orbit completed 1.55 revolutions around the inner cylinder for each revolution around the vortex center, while a particle on the innermost orbit needed only 0.33 revolutions around the cylinder for each revolution around the vortex center.

If the particles are more dense than the fluid, gravity can play a significant role in the particle motion. Figure 2 shows the projection of the particle paths in a meridional plane for three different density ratios with gravity acting downward, parallel to the axis of rotation. The ratio of the gravitational force to the centrifugal acceleration is 245, typical of that used in our large-scale laboratory rotating filter device, but much larger than that in commercial devices for blood plasma separation. The upper and lower boundaries of the figure are periodic, so that particles that exit the bottom of the figure at $z/d=0$ reenter the top of the figure at $z/d=2\pi/kd=2.007$. There are two vortices in this figure, the top one rotating clockwise and the bottom one rotating counterclockwise. The density ratio always appears as $(\beta-1)$ in the force balance equation, so results for $\beta=1.01, 1.10, 2.00$ represent a two orders of magnitude increase in $(\beta-1)$. Figure 2(a) shows that nearly neutrally buoyant particles are largely caught up in the vortices. A few of the particles wind downward around the vortices. Although it is difficult to detect in Fig. 2(a), the paths of particles caught in the vortices are not closed loops, but over long times spiral inward or outward, as discussed later in this paper.

Increasing the particle density relative to the fluid density results in more particles winding around vortices while generally moving downward, as shown in Fig. 2(b). Other particles remain bound up in nearly closed particle paths in "retention zones." Even though the vortices extend across the entire annular gap, the retention zones are alternately close to the inner and outer wall of the annulus. The particles that wind downward around the vortices are caught in the downward axial motion on the side of one vortex. Then they fall by gravity into the next vortex, where they continue their downward axial motion on the opposite side of that vortex.

A further increase in the particle density results in wavy axial particle paths, shown in Fig. 2(c). The waviness results from the Taylor vortices carrying the particles radially, but the difference in the density between the particles and the fluid is so large that particles fall right through a vortex without being caught up in the vortical flow. For the particles closest to the inner cylinder, several parallel particle paths are evident. This results from the generally outward radial motion of the particles due to the centrifugal force and the periodic boundary condition imposed in the analysis. For instance, the particle associated with the innermost path moves downward and a small distance radially outward so that when it reenters the periodic domain at the top of the figure, its path is at a slightly greater radius. As a result, a particle-free zone will tend to form near the inner cylinder. A similar effect occurs for smaller values of β , although it is not readily apparent from the particle paths in Fig. 2(a). Near the fixed outer cylinder, the centrifugal force is negligible, so the particle paths overlap in Fig. 2(c). Since the radial velocity due to the vortices is greatest away from the walls of the annulus, the particle paths are wavy near the center of the annulus. The particle paths in Fig. 2 are in qualitative agreement with the results of Rudman *et al.*¹¹

It is clear from Fig. 2 that gravity plays a major role in defining paths for non-neutrally buoyant particles by carrying particles axially from one vortex to another, but our primary interest here is in the relative effect of the other forces on the motion of particles. In particular, we are interested in the relative importance of the centrifugal acceleration and the drag due to the Taylor vortices on particle motion. To study this interplay of forces, it is helpful to remove the gravitational field from the analysis in order to compare the more subtle effects of other forces on the particle motion. Furthermore, the motion of particles in a gravity-free environment, germane to the use of rotating filters for water purification in outer space applications, is of interest. Consequently, the gravitational force has been set to zero for the following results.

Nonwavy Taylor vortices are independent cells with no cross-flow between vortices. Thus, the streamlines for axisymmetric Taylor Couette flow are closed. When the gravitational force is zero and diffusion is omitted, particles will not cross from one vortex into another. The projection in a meridional plane of two particle paths in a single counter-clockwise vortex are shown in Fig. 3 for relatively dense particles ($\beta=11$). A particle that begins near the inner cylinder at $[r/d \approx 4.94, z/d \approx 0.42]$ spirals inward toward the vortex center. A particle that begins near the center of the vortex

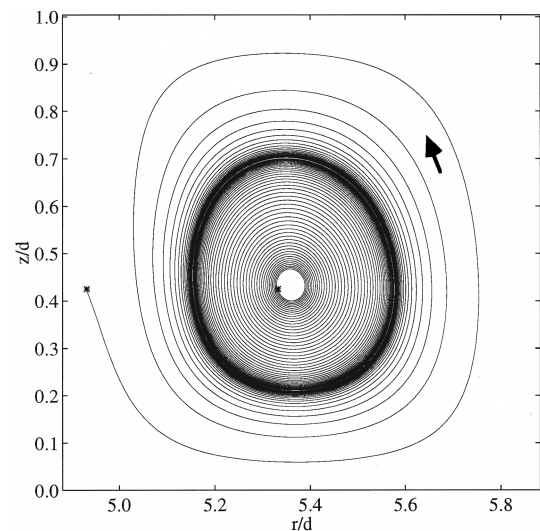


FIG. 3. Particle paths projected in the meridional plane with no gravitational body force for $Re=125$, $\alpha=29.7$, and $\beta=11$. The asterisks mark the starting point. The dark orbit is the limit cycle.

at $[r/d=5.33, z/d \approx 0.42]$ spirals outward from the vortex center. Clearly both particles approach a limit cycle indicated by the dark band between the two spiral paths. (The actual limit cycle orbit is a single path. The dark band results from plotting the closely spaced particle paths as they slowly approach the limit cycle orbit.) Based on the spiral nature of either particle path, it is evident that particles initially at other locations in the flow domain will also eventually end up on the same final orbit. Because of the nature of Taylor vortex flow, the particle paths for the adjacent vortices above or below the vortex shown would be mirror images reflected about the boundary between the vortices.

Limit cycles similar to those shown in Fig. 3 occur over two orders of magnitude decrease in $(\beta-1)$, as shown in Fig. 4. As the density ratio decreases, the particles spiral toward the limit cycle much more slowly. The overlap of the limit

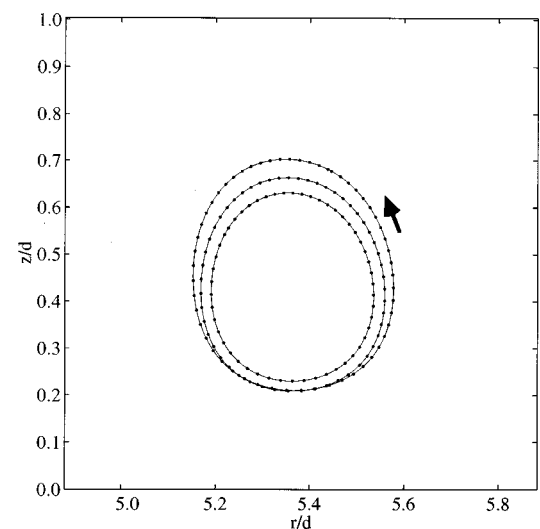


FIG. 4. Limit cycle orbits with no gravitational body force for $Re=125$, $\alpha=29.7$, and $\beta=1.1, 2, 11$ (from smallest to largest). Dots on the curve are equally spaced in time.

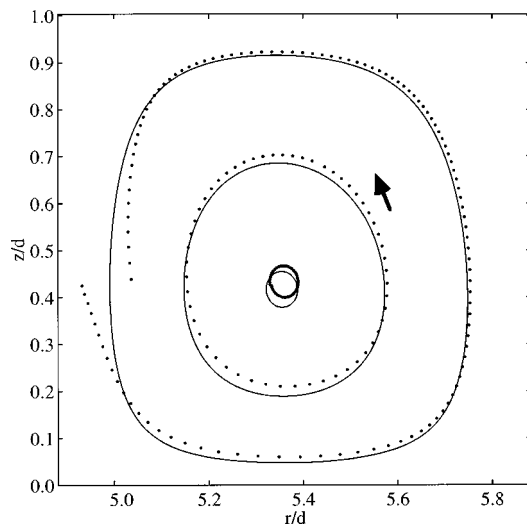


FIG. 5. Particle paths (dots) and streamlines (solid curves) for $Re=125$, $\alpha=29.7$, and $\beta=11$ with no gravitational body force. Dots are equally spaced in time.

cycle paths for $\beta=2$ and 11 in the outflow region is somewhat surprising. We have checked this result thoroughly and concluded that it is coincidental, resulting from the interaction of the drag force and the sedimentation force in each case.

The particle paths approximately follow the vortical flow, but the paths deviate slightly from the streamlines as shown in Fig. 5. In this figure, three particle paths are shown (in order of decreasing diameter): spiraling inward, limit cycle, and spiraling outward. In each case, the particle path is indicated by the dots corresponding to uniform time increments. The solid curve represents the streamline that corresponds to the best fit streamfunction (in a least-squares sense) to the particle path. Consider first the largest diameter path. The particle begins near the inner cylinder. The higher density particle sediments radially outward past the streamline due to the centrifugal field so that the particle is radially outside of the streamline when it nears the outer cylinder. But as the particle gets closer to the outer cylinder, the centrifugal force decreases and the fluid drag due to the vortex motion becomes large enough to overcome the small centrifugal force, bringing the particle back toward the inner cylinder. Near the inner cylinder, the outward centrifugal force increases, preventing the particle from reaching its initial radial position. Thus, as the vortex carries the particle around one orbit, the diameter of the orbit decreases causing the particle to spiral toward the limit cycle orbit. Near the center of the vortex the centrifugal field is not as strong. As a result, the fluid drag due to the vortex motion carries the particle a little farther inward than the centrifugal force sediments the particle outward, resulting in the particle spiraling toward the larger diameter limit cycle orbit. The change in radius of the smallest diameter path during one cycle is so small that it is not easily evident in Fig. 5. For the closed orbit, the inward deviation of the particle path from the streamline is the same as its outward deviation from the streamline, resulting in a particle following a limit cycle orbit.

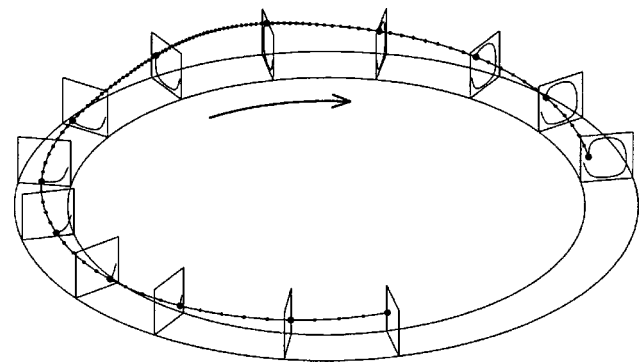


FIG. 6. The three-dimensional particle path for the particle in the outermost orbit in Fig. 5. Dots on the curve are equally spaced in time.

Although Fig. 5 shows the particle path in the meridional plane, the particle is also simultaneously moving azimuthally. A three-dimensional representation of the path of the particle on the outermost orbit in Fig. 5 with dots representing identical time steps is shown in Fig. 6 as the particle revolves clockwise around the inner cylinder. The spacing between dots shows that the azimuthal particle velocity is quite high near the inner cylinder and quite low near the outer cylinder. The particle quickly moves from its initial position near the inner cylinder into the outflow region between the vortex shown and the next lower vortex. As it moves outward it slows and then spends substantial time moving axially near the outer cylinder. It accelerates azimuthally as it moves inward toward the inner cylinder and finally ends its revolution about the vortex center closer to the center than where it started.

The particle on the outermost orbit completes 0.80 revolutions around the inner cylinder for each revolution around the vortex center, while a particle on the limit cycle path needs only 0.40 revolutions around the cylinder to complete each orbit. Thus, a particle on the limit cycle orbit would move around that orbit about 2.5 times for every time it makes one complete revolution in the annulus. The density of the particle is of little consequence for the azimuthal motion. This is most evident for the smallest diameter paths in Figs. 1 and 5. These two paths are essentially the same diameter and extend azimuthally 0.33 revolutions around the cylinder for the neutrally buoyant particle and 0.32 revolutions around the cylinder for the more dense particle for each revolution around the vortex center.

The motion of the particle comes about as a result of the relative importance of the various terms of Eq. (2). These terms are shown in Fig. 7 as a function of time over the limit cycle period, T , for $Re=125$. The upper part of Fig. 7 shows the radial position of the particle through one complete orbit, with the particle being at its nearest approach to the inner cylinder at $t/T=0$ and 1. The curves in the lower part of Fig. 7 show the relative magnitude of the radial components of the particle inertia, centrifugal force, drag force, and the pressure gradient force throughout one orbit around the limit cycle path, where the forces F are nondimensionalized using the speed of the inner cylinder $r_i\Omega$, the gap width d , and the particle mass m_p . It is evident that the largest forces are

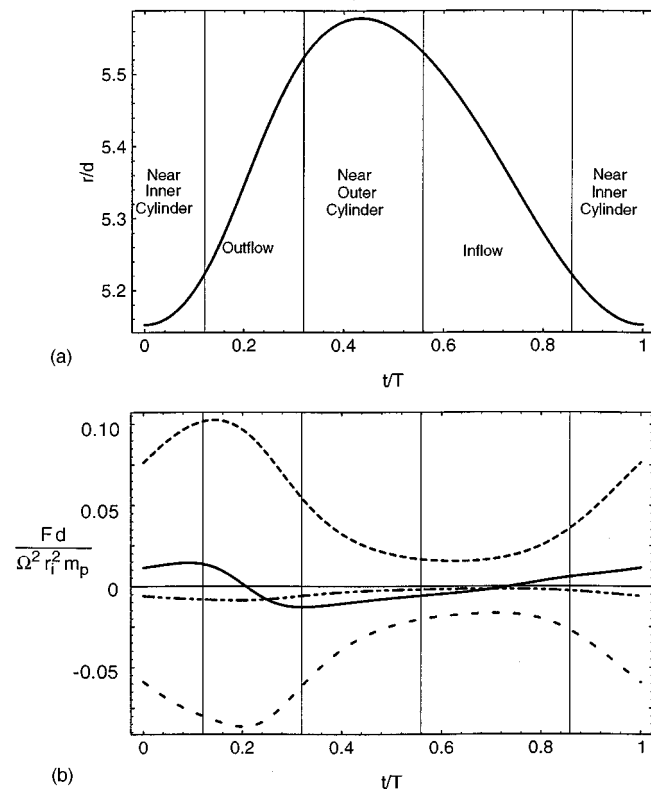


FIG. 7. (a) The particle position as a function of time. (b) The dimensionless radial forces and inertia of a particle on a limit cycle orbit $Re=125$, $\alpha=29.7$, and $\beta=11$ as a function of time. —, inertia; ---, centrifugal force; - - -, drag force, ----, pressure gradient force. The gravitational body force is omitted.

those related to the centrifugal field and the drag on the particle. The pressure gradient force is much smaller, but is the same order of magnitude as the resulting inertia. The acceleration due to the added mass is quite small, about two orders of magnitude less than the force due to the pressure gradient, so it overlays the horizontal axis in the figure.

The minimum centrifugal force occurs slightly after the particle reaches its outermost radial position, and the maximum centrifugal force occurs slightly after the particle reaches its innermost radial position. The lag of the particle centrifugal force behind the fluid centrifugal acceleration is related to the different azimuthal velocities of the particle and the fluid. It takes some time for the particle to reach the same local azimuthal velocity as the fluid, resulting in the phase lag. Contributing to this effect is the transport of low momentum fluid inward at the inflow boundaries between vortices and the transport of high momentum fluid outward at the outflow boundaries.²³ For instance, in an outflow boundary, the particle can travel radially outward in a region of high azimuthal velocity to quite near the outer cylinder before the azimuthal fluid velocity decreases substantially. Thus, the particle can be well past its outermost radial position before its azimuthal velocity and, consequently, the centrifugal force have decreased to their minimum values.

When the particle is moving axially near the inner cylinder, $0.00 < t/T < 0.12$ and $0.86 < t/T < 1.00$, it acquires a high azimuthal velocity resulting in an increase in the centrifugal force acting on the particle after a short lag. As the

particle is carried outward in an outflow region between vortices, $0.12 < t/T < 0.32$, the centrifugal force results in the particle traveling radially outward faster than the surrounding fluid eventually causing a radially inward drag force on the particle. When the particle is moving axially near the outer cylinder, $0.32 < t/T < 0.56$, it loses its azimuthal velocity so the outward centrifugal force is subsequently reduced. By the time the particle is in the inflow region between vortices, $0.56 < t/T < 0.86$, its azimuthal velocity is small, so the outward directed centrifugal force is small. The particle is moving inward more slowly than the surrounding fluid, so the drag force is directed inward, causing the particle to move radially inward. Of course, the particle eventually nears the inner cylinder, where it regains its azimuthal velocity and the cycle repeats.

When a particle is outside of the limit cycle orbit, the radially inward drag force and pressure gradient force during each revolution are never quite enough to carry the particle back to its original radial position near the inner cylinder, and the particle spirals inward toward the vortex center to its limit cycle orbit. When the particle is inside of the limit cycle orbit, the inward drag force and pressure gradient force during each revolution always carry the particle radially inward to a smaller radial position than for its previous orbit, and the particle spirals outward from the vortex center to its limit cycle orbit. In the limit cycle orbit, the net outward centrifugal force is just balanced by the net inward drag and pressure gradient forces to bring the particle back to its original starting position after each orbit.

IV. MOTION OF PARTICLES WITH AN IMPOSED RADIAL FLOW

The original motivation for this work was to understand the motion of particles in a rotating filter separator in which the inner cylinder is a filter through which fluid, but not particles, can pass. In a rotating filter, an axial flow in the annulus provides the source of fluid that flows radially inward through the inner porous cylinder. It is quite difficult to model this flow analytically, although some progress has been made in that direction.^{9,27} Instead, we use a simple, *ad hoc* approach to shed light on the effect of a radial inflow on particle motion. We form an approximate solution to the equations of motion by adding a small continuity-satisfying radial inflow (from the outer cylinder to the inner cylinder) to the Davey solution. This is equivalent to making both the inner and outer cylinders porous. This flow, while clearly not identical to that in a rotating filter, can provide insight into how particle motion, particularly near the inner cylinder, in Taylor Couette flow can be affected by a radial flow. We can confidently add a small radial flow without significantly altering the Taylor vortices based on stability analyses that indicate that the transition Reynolds number, transition wave number, and perturbation velocities are virtually unaffected for small radial Reynolds numbers.^{28,29}

Including a small radial throughflow does not change the azimuthal or axial velocity, to a first approximation, from that given by Eqs. (1b) and (1c). The radial velocity is altered slightly to

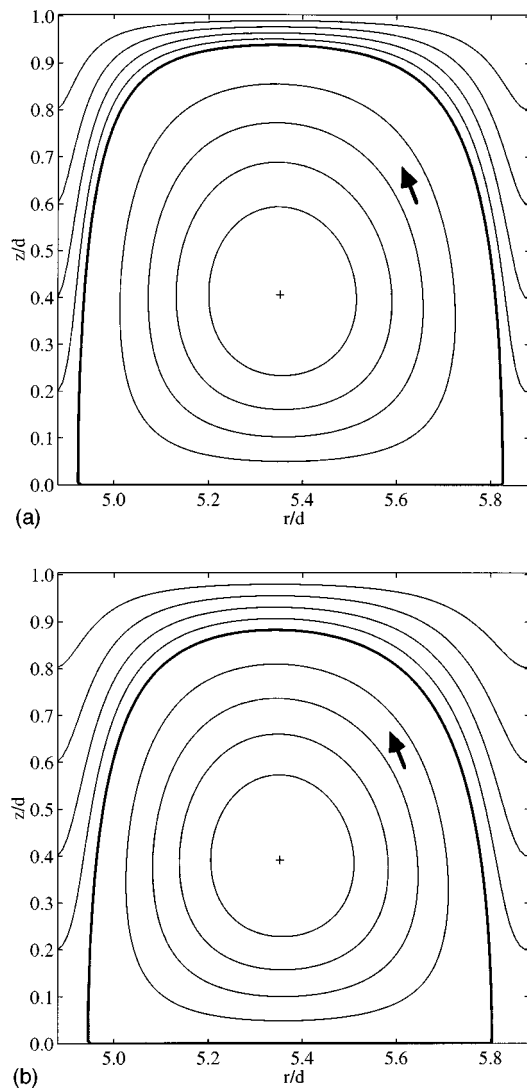


FIG. 8. Streamlines for the Davey solution for a CCW vortex, $Re=125$, with an imposed right to left radial throughflow. The vortex centers are marked with a plus (+) symbol. Each set of streamlines, both inside and outside the heavy streamline, are spaced equally although the spacing inside is not equal to the spacing outside. (a) $Re_{rad}=0.1$; (b) $Re_{rad}=0.2$.

$$u_r(r, z, \epsilon', Re_{rad}) = u_r(r, z, \epsilon') + \frac{Re_{rad}}{Re} \frac{r_i}{r}, \quad (3)$$

where $u_r(r, z, \epsilon')$ is the radial velocity from the Davey solution [Eq. (1a)] and $Re_{rad} = u_{r,i} d / \nu$ is the radial Reynolds number based on the radial velocity at the inner cylinder $u_{r,i}$ and the gap width d . Since the second term on the right-hand side of (3) satisfies continuity, the radial velocity including the Davey solution and the radial throughflow exactly satisfies continuity. For typical conditions of Re_{rad} of $O(0.1)$ or smaller and Re of $O(100)$, the second term on the right-hand side is easily small enough to be considered a perturbation to the flow. Thus, momentum conservation is also satisfied to leading order.

The streamlines of the vortical flow with the imposed radial flow at two radial Reynolds numbers are shown in Fig. 8 for a single counterclockwise vortex at $Re=125$. The perturbed velocity field retains the reflectional symmetry about

the outflow boundary (at $z/d=0$) of the original Davey solution. The bold curve represents the boundary streamline between fluid elements that are trapped in the vortex and those that proceed from right to left (from the outer cylinder to the inner cylinder) around the vortex. It is evident that increasing the radial flow causes more fluid to be swept inward to the inner cylinder and less to be retained in the vortex. The area within the bold boundary streamline is about three-quarters of the total area of the vortex cell for $Re_{rad}=0.1$, while it is about two-thirds for $Re_{rad}=0.2$.

Neutrally buoyant particles would follow the streamlines shown in Fig. 8 fairly closely, except for the small deviations due to the velocity field curvature near the particles similar to that indicated in Fig. 1. However, particles that are more dense than the fluid are subject to a centrifugal force that acts to carry them outward against the radial flow. Simulating the motion of such particles begins with the particles initially advecting with the vortical flow and then suddenly switching on the radial flow. In this case we consider particles only slightly more dense than the fluid, $\beta=1.01$. Results of the simulation at two radial Reynolds numbers with no gravitational body force are shown in Fig. 9 for ten particles, started at evenly spaced positions along a vertical line near the outer cylinder (marked with asterisks). Four additional particles were started within the heavy streamline that marks the boundary between fluid elements that are trapped in the vortex and fluid elements outside of the vortex. All particles that were started within the bold streamline complete orbits within the ‘‘retention zone,’’ and are thus prevented from getting near enough to the inner cylinder to have potential to foul it. Assuming an approximately uniform initial particle concentration, the fraction of particles remaining in the retention zone is approximately equivalent to the area of the retention zone: about three-quarters for $Re_{rad}=0.1$ and two-thirds for $Re_{rad}=0.2$. Since the particles are only slightly more dense than the fluid, there is no evidence of spiraling toward a limit cycle orbit over the duration of the simulation. Over a long time, such spiraling toward a limit cycle does occur.

The particles that were started outside of the retention zone near the outer cylinder are carried upward and then radially inward. For $Re_{rad}=0.1$, seven out of the ten particles are carried around the vortex and then downward before they reach the inner cylinder, as shown in Fig. 9(a). In a physical device, these particles get near enough to the porous inner cylinder to have potential for fouling it, although other effects such as the filtration membrane surface chemistry and morphology as well as inertial particle migration, none of which are not included in our model, clearly can play a significant role in the fate of these particles. Three out of the ten particles outside of the ‘‘retention zone’’ never reach the inner cylinder and are captured by the vortex, spiraling toward the limit cycle orbit within the retention zone. Their paths are evident near the bottom corners of the bold streamline. Smaller radial flows would result in more particles being captured in the retention zone.

At a larger radial Reynolds number, $Re_{rad}=0.2$, all of the particles that started near the outer cylinder reach the inner cylinder, as shown in Fig. 9(b). In this case, the particles are

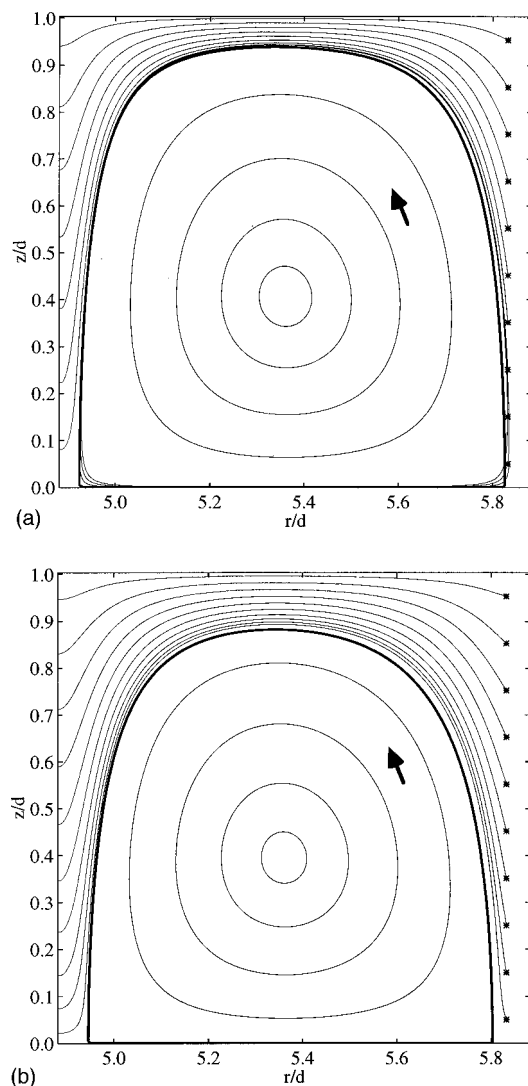


FIG. 9. Particle paths for $Re=125$, $\alpha=29.7$, and $\beta=1.01$, with an imposed right to left radial throughflow and no gravitational body force. The asterisks (*) represent the starting positions of some of the particles. The four closed curves show the paths of four particles trapped by the vortex. The heavy curve is the streamline that separates trapped fluid elements from fluid elements added and removed by the radial flow. (a) $Re_{rad}=0.1$; (b) $Re_{rad}=0.2$.

subject to a larger radial drag force and they are exposed to the centrifugal field for a shorter time than at the lower radial Reynolds number because of the higher imposed radial velocity. As a result, fewer particles will be trapped in the vortex and more particles can potentially deposit in the pores of the porous inner cylinder. Even so, the majority of particles will remain trapped in the vortex, away from the inner cylinder in the retention zone. Of course, at a high enough radial velocity no particles will be trapped in the vortex and the limit cycle path will not occur because the drag related to the radial flow will overwhelm centrifugal force on the particles. In this case, the particles will all end up at the inner cylinder.

V. DISCUSSION

The goal of this research was to obtain insight into the physical mechanism that causes the segregation of particles

in supercritical Taylor Couette flow. These same mechanisms can contribute to the observed antiplugging behavior of rotating filter separators. Neutrally buoyant particles nearly follow the fluid streamlines, with only small deviations due to the Faxen correction in the force balance on a particle. But for particles with a density greater than the fluid, the situation in most rotating filter applications, the particle paths deviate substantially from the fluid streamlines due to the interplay between the centrifugal force and the drag force. Particles near the center of a vortex spiral outward seeking a limit cycle orbit that is not near the walls of the annulus. Likewise particles far from the center of the vortex spiral inward seeking the same limit cycle orbit. We have observed the concentration of particle image velocimetry (PIV) tracer particles away from the walls of the annulus in a Taylor Couette cell after several hours of operation, consistent with the predicted limit cycle behavior. Other researchers have noted a similar result.³⁰ Since the forces on the particles tend to keep them away from the inner cylinder, the tendency toward a limit cycle orbit appears to be a key factor related to the antiplugging character of rotating filtration.

Of course, in a rotating filter there is a small radial flow through the porous inner cylinder which causes an additional radially inward drag force on the particles very near the inner cylinder that could draw particles toward the pores of the inner cylinder and cause plugging. But modeling this velocity as a radially inward throughflow indicates that this radial velocity is not strong enough to carry a substantial number of particles to the inner cylinder. Most particles remain in orbits within the vortex retention zone. Only a small fraction of particles are likely to get close enough to the filter to plug its pores. Even in the presence of gravity, it appears that the interplay between the centrifugal force and the drag force is likely to play a major role in preventing particles from getting near the porous inner cylinder and plugging its pores.

ACKNOWLEDGMENTS

This work was supported by the National Science Foundation Grant No CTS-9400033. A brief, preliminary paper³¹ based on this research was published by the American Society of Mechanical Engineers (ASME), which has granted permission for the publication of this paper.

¹R. M. Lueptow, "Fluid mechanics of a rotating filter separator," in *Advances in Filtration and Separation Technology*, edited by K. J. Choi (American Filtration and Separations Society, Northport, AL, 1995), Vol. 9, pp. 283–291.

²J. R. Hildebrandt and J. B. Saxton, "The use of Taylor vortices in protein processing to enhance membrane filtration performance," in *Bioprocess Engineering Colloquium*, edited by R. C. Dean and R. M. Nerem (The American Society of Mechanical Engineers, New York, 1987), pp. 93–95.

³G. Belfort, R. H. Davis, and A. L. Zydney, "The behavior of suspensions and macromolecular solutions in crossflow microfiltration," *J. Membr. Sci.* **96**, 1 (1994).

⁴B. Hallstrom and M. Lopez-Leiva, "Description of a rotating ultrafiltration module," *Desalination* **24**, 273 (1978).

⁵K. Ohashi, K. Tashiro, F. Kushiya *et al.*, "Rotation-induced Taylor vortex enhances filtrate flux in plasma separation," *Trans. Am. Soc. Artif. Intern. Organs* **34**, 300 (1988).

⁶G. Beaudoin and M. Y. Jaffrin, "Plasma filtration in Couette flow membrane devices," *Artif. Organs* **13**, 43 (1989).

- ⁷K. H. Kroner and V. Nissinen, "Dynamic filtration of microbial suspensions using an axially rotating filter," *J. Membr. Sci.* **36**, 85 (1988).
- ⁸U. B. Holeschovsky and C. L. Cooney, "Quantitative description of ultrafiltration in a rotating filtration device," *AIChE J.* **37**, 1219 (1991).
- ⁹G. Belfort, J. M. Pimbley, A. Greiner, and K. Y. Chung, "Diagnosis of membrane fouling using a rotating annular filter. 1. Cell culture media," *J. Membr. Sci.* **77**, 1 (1993).
- ¹⁰G. Belfort, P. Mikulasek, J. M. Pimbley, and K. Y. Chung, "Diagnosis of membrane fouling using a rotating annular filter. 2. Dilute particle suspensions of known particle size," *J. Membr. Sci.* **77**, 23 (1993).
- ¹¹M. Rudman, K. Hourigan, and M. Thompson, "Particle shear-rate history in a Taylor-Couette column," in *Liquid-Solid Flows*, edited by M. C. Roco, C. T. Crowe, D. D. Joseph *et al.* (ASME, New York, 1994), Vol. FED. 189, pp. 22-29.
- ¹²M. Rudman, "Mixing and particle dispersion in the wavy vortex regime of Taylor-Couette flow," *AIChE J.* **44**, 1015 (1998).
- ¹³R. M. Lueptow and A. Hajiloo, "Flow in a rotating membrane plasma separator," *ASAIO J.* **41**, 182 (1995).
- ¹⁴S. T. Wereley and R. M. Lueptow, "Spatio-temporal character of supercritical circular Couette flow," *J. Fluid Mech.* **364**, 59 (1998).
- ¹⁵H. A. Snyder, "Experiments on the stability of spiral flow at low axial Reynolds numbers," *Proc. R. Soc. London, Ser. A* **265**, 198 (1962).
- ¹⁶K. C. Chung and K. N. Astill, "Hydrodynamic instability of viscous flow between rotating coaxial cylinders with fully developed axial flow," *J. Fluid Mech.* **81**, 641 (1977).
- ¹⁷D. I. Takeuchi and D. F. Jankowski, "A numerical and experimental investigation of the stability of spiral Poiseuille flow," *J. Fluid Mech.* **102**, 101 (1981).
- ¹⁸R. M. Lueptow, A. Docter, and K. Min, "Stability of axial flow in an annulus with a rotating inner cylinder," *Phys. Fluids A* **4**, 2446 (1992).
- ¹⁹A. Davey, "The growth of Taylor vortices in flow between rotating cylinders," *J. Fluid Mech.* **14**, 336 (1962).
- ²⁰J. P. Gollub and M. H. Freilich, "Optical heterodyne test of perturbation expansions for the Taylor instability," *Phys. Fluids* **19**, 618 (1976).
- ²¹T. Berland, T. Jøssang, and J. Feder, "An experimental study of the connection between the hydrodynamic and phase-transition descriptions of the Couette-Taylor instability," *Phys. Scr.* **34**, 427 (1986).
- ²²R. M. Heinrichs, D. S. Cannell, G. Ahlers, and M. Jefferson, "Experimental test of the perturbation expansion for the Taylor instability at various wavenumbers," *Phys. Fluids* **31**, 250 (1988).
- ²³S. T. Wereley and R. M. Lueptow, "Azimuthal velocity in supercritical circular Couette flow," *Exp. Fluids* **18**, 1 (1994).
- ²⁴M. R. Maxey and J. J. Riley, "Equation of motion for a small rigid sphere in a nonuniform flow," *Phys. Fluids* **26**, 883 (1983).
- ²⁵J. B. McLaughlin, "Inertial migration of a small sphere in linear shear flows," *J. Fluid Mech.* **224**, 261 (1991).
- ²⁶A. J. Goldman, R. G. Cox, and H. Brenner, "Slow viscous motion of a sphere parallel to a plane wall—I. Motion through a quiescent fluid," *Chem. Eng. Sci.* **22**, 637 (1967).
- ²⁷F. Marques, J. Sanchez, and P. D. Weidman, "Generalized Couette-Poiseuille flow with boundary mass transfer," *J. Fluid Mech.* **347**, 221 (1998).
- ²⁸K. Min and R. M. Lueptow, "Hydrodynamic stability of viscous flow between rotating porous cylinders with radial flow," *Phys. Fluids* **6**, 144 (1994).
- ²⁹E. C. Johnson and R. M. Lueptow, "Hydrodynamic stability of flow between rotating porous cylinders with radial and axial flow," *Phys. Fluids* **9**, 3687 (1997).
- ³⁰M. A. Dominguez-Lerma, G. Ahlers, and D. S. Cannell, "Effects of Kaliloscope flow visualization particles on rotating Couette-Taylor flow," *Phys. Fluids* **28**, 1204 (1985).
- ³¹S. T. Wereley and R. M. Lueptow, "Particle motion in Taylor Couette flow," in *Proceedings of the ASME Ocean Engineering Division*, edited by D. T. Valentine and C. C. Jahnke (ASME, New York, 1997), Vol. OED-14, pp. 73-79.